Molecular Crystals and Liquid Crystals

ISSN: 1542-1406 (Print) 1563-5287 (Online) Journal homepage: http://www.tandfonline.com/loi/gmcl20

Three-Dimensional Analysis of the Autostereoscopic Display with an Array of Lenticulars

Bong-Sik Kim, Seung-Chul Lee, Keon-Woo Kim & Woo-Sang Park

To cite this article: Bong-Sik Kim, Seung-Chul Lee, Keon-Woo Kim & Woo-Sang Park (2015) Three-Dimensional Analysis of the Autostereoscopic Display with an Array of Lenticulars, Molecular Crystals and Liquid Crystals, 612:1, 46-55, DOI: 10.1080/15421406.2015.1030573

To link to this article: http://dx.doi.org/10.1080/15421406.2015.1030573

Published online: 06 Jul 2015.

Mol. Cryst. Liq. Cryst., Vol. 612: pp. 46–55, 2015

ISSN: 1542-1406 print/1563-5287 online
DOI: 10.1080/15421406.2015.1030573

Taylor & Francis
Taylor & Francis Group

Three-Dimensional Analysis of the Autostereoscopic Display with an Array of Lenticulars

BONG-SIK KIM, SEUNG-CHUL LEE, KEON-WOO KIM, AND WOO-SANG PARK*

Department of Electronics Engineering, Inha University, Incheon, Korea

Three-dimensional analysis of the optical functionalities of an autostereoscopic display with an array of slanted lenticular lenses was performed. The specification parameters of the lenticular lens for clear separation of the images were first determined using the geometrical optics, and the transmission characteristics of the light ray travelling through a single lenticular were then calculated by finite ray tracing. The properties of light transmission over the entire display panel were then determined by expanding the results obtained for the single lenticular to the entire lenticular lens array. Consequently, each view was confirmed to be located at an interocular distance of 65 mm *away from each other. Approximately 5% noise was observed between the views, and the shape of the viewing zone at the optimal viewing distance was tilted towards the direction of the slanted lenticular. Overall, numerical analysis enables a realistic evaluation of the optical functionalities, such as the shape of the viewing zone, of lenticular based autostereoscopic displays.*

Keywords autostereoscopic display; lenticular; finite ray tracing

Introduction

Autostereoscopic displays that provide three-dimensional(3D) images without special glasses have attracted considerable attention because of the significant improvement in their image quality. Spatial multiplex technology is one of the key autostereoscopic display technologies, where an optical filter, such as a parallax barrier or an array of cylindrical lenses, i.e., lenticulars, is attached to the front of a display panel to generate parallax images [1–3]. The parallax barrier method is simple and easy to realize, but its slit structure leads to significant light loss. On the other hand, the lenticular approach provides good image quality and light efficiency by projecting the left and right pixel images directly to the corresponding eyes. In particular, an autostereoscopic display with slanted lenticulars has been reported to exhibit excellent image quality by eliminating the Moiré-like effect. The performance of autostereoscopic displays is generally evaluated by the capability to

*Address correspondence to Woo-Sang Park, Department of Electronics Engineering, Inha University, 100 Inha-ro, Incheon 402-751, Korea. E-mail: wspark@inha.ac.kr

Color versions of one or more of the figures in the article can be found online at www.tandfonline.com/gmcl.

Table 1. Specification parameters of the display panel with an array of lenticular lenses used in the simulation

Liquid Crystal Display		Lenticular Lens	
Parameters	Values	Parameters	Values
Panel Size	4.5 *inch*	Number of View	2
Resolution	1280×720	Slant Angle	18.4°
Pixel Structure	RGB stripe	Focal Length	112.5 μm
Pixel Pitch	77.1 μm	Lens Pitch	51.3 μm

separate the views. As the crosstalk between the views is minimized, the viewer can experience even clearer images. Recently, some studies have evaluated the image quality of 3D displays at an optimal viewing distance using the crosstalk or noise between the images for the left and right eyes [4–9]. Most simulations for autostereoscopic 3D displays, however, have used two-dimensional analysis, which cannot evaluate the noise level and distortion of the viewing zone caused by slanting the lenticulars.

In this study, three-dimensional analysis of lenticular based autostereoscopic 3D displays was performed using geometrical optics to evaluate their optical functionalities. To obtain clear images, the slant angle of the lenticular lens was first calculated by considering the configuration of the pixels and the pixel pitch. The key specification parameters of the lenticular lens, such as the lens pitch, radius of curvature and focal length, were then determined using geometrical optics. Based on the results, numerical simulations were carried out throughout the display panel by finite ray tracing to enable fast and accurate calculations. This study finally confirmed whether a 3D image could be realized and evaluated the quality of the 3D images produced using the noise level.

Design Logics and Simulation Details

Table 1 lists the specification parameters of the display panel with an array of lenticulars used in the simulation. The parameters related to the lenticular lens were calculated from geometrical optics by considering the resolution of the panel, the configuration of the pixels, pixel pitch, and slant angle [10–11].

For the optimized lens listed in Table 1, the optical transmission characteristics of a single lenticular lens were calculated and a three-dimensional simulation was performed by expanding the calculation results to the entire display panel with an array of lenticulars. The following gives a brief description of the computational logic used. The center of curvature of the slanted lenticular lens was first calculated from that of a non-slanted lenticular lens and slant angle. Using the equation of the cylinder centered on the center of curvature obtained above, the emergent point on the lenticular surface of the slanted lens, corresponding to the incident point of the light ray incident on the base of the lens, was then calculated. For simplicity, the incident and emergent points on the slanted lenticular were replaced with the corresponding points on the spherical lens, and finite ray tracing was carried out to obtain the directional cosines of the emergent light rays corresponding to the incident light rays. By rotating the directional cosine of the emergent ray from the spherical lens by the slant angle, that of the emergent ray from the slanted lenticular was

calculated. The computational results for the single lenticular were finally expanded to the entire array of lenticulars.

Figure 1 presents a schematic drawing of the lenticulars used in the simulation. As depicted in the figure, lenticulars, which are composed of cylindrical lenses, were arrayed periodically in columns with a pitch of P. R represents the radius of the lenticular lens. S denotes the distance from the center of curvature to the base of the lens. l stands for the order of a single lens in an array of lenticulars. The lens placed just on the center of the display panel was numbered 0, those on its left and right sides were numbered -1 and $+1$, respectively, the next left and right ones were numbered -2 and $+2$, respectively, and so on. The light ray incident at point (x_r, y_r, z_r) on the base of the lenticular lens with inclination and azimuth angles (θ_i, ϕ_i) travels by a distance of t through the lens with the angles (θ_r, ϕ_r) according to Snell's law and arrives at point (x_e, y_e, z_e) on the lenticular surface. The light ray reaching the lenticular surface is then refracted into air at angles (θ_e, ϕ_e) relative to the normal.

The coordinate of the center of curvature for the slanted lens, $\left(x', y', z'\right)_{CC}$, is expressed using that of the non-slanted lens, $(x, Pl, -S)_{CC}$ as follows:

$$\begin{pmatrix} x' \\ y' \\ z' \end{pmatrix}_{CC} = \begin{pmatrix} \cos\phi_s & -\sin\phi_s & 0 \\ \sin\phi_s & \cos\phi_s & 0 \\ 0 & 0 & 1 \end{pmatrix} \begin{pmatrix} x \\ Pl \\ -S \end{pmatrix}_{CC} = \begin{pmatrix} x\cos\phi_s - Pl\sin\phi_s \\ x\sin\phi_s + Pl\cos\phi_s \\ -S \end{pmatrix}, \quad (1)$$

where ϕ_s is the slant angle. The emergent point on the slanted lenticular surface was obtained using the equation of the cylinder. The equation representing the non-slanted lenticular surface can be assumed to be identical to the equation of the cylinder. In the case of the slanted lenticular, however, the equation of the lenticular surface needs to be modified to take the slant angle into consideration. Using the center of curvature in Eq. (1),

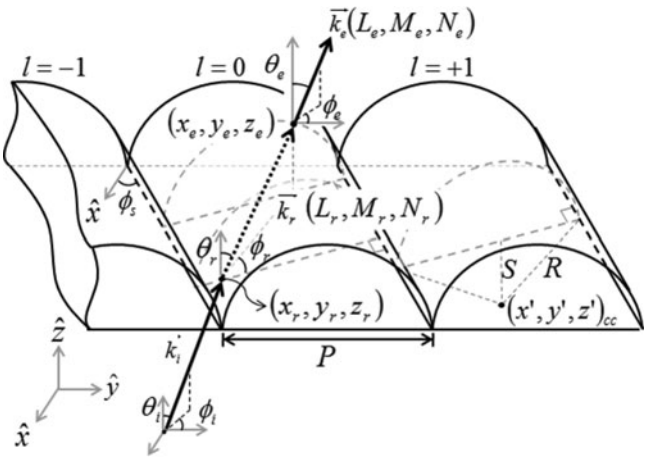

Figure 1. Schematic diagram of the lenticulars. The solid and dotted lines indicate the cross sections perpendicular to the x-axis and to the direction along the length of the lens, respectively. The lenticulars, composed of cylindrical lenses, are arrayed periodically in columns with a pitch of P. The light ray is incident on the base of the lenticular lens, is refracted into the lens, and then emerges from the surface of the lens. $\vec{k}_i$, $\vec{k}_r$, and $\vec{k}_e$ denote the wavevectors of the incident, refracted, and emergent light rays, respectively.

the slanted lenticular surface can be expressed as

$$f(x_e, y_e, z_e) = (x_e \sin\phi_s + y_e \cos\phi_s - Pl)^2 + (z_e + S)^2 - R^2 = 0. \tag{2}$$

Here, the three unknowns, i.e. the emergent point (x_e, y_e, z_e), can be also written as

$$\begin{aligned} x_e &= t \sin\theta_r \cos\phi_r + x_r, \\ y_e &= t \sin\theta_r \sin\phi_r + y_r, \\ z_e &= t \cos\theta_r. \end{aligned} \tag{3}$$

Solving for the propagation distance t, after substituting Eq. (3) into Eq. (2), gives the following:

$$\begin{aligned} t &= \frac{-\beta + \sqrt{\beta^2 - \alpha\gamma}}{\alpha}, \\ \alpha &= \sin^2\theta_r \sin^2(\phi_s + \phi_r) + \cos^2\theta_r, \\ \beta &= \sin\theta_r \sin(\phi_s + \phi_r)(x_r \sin\phi_s + y_r \cos\phi_s - Pl) + S\cos\theta_r, \\ \gamma &= (x_r \sin\phi_s + y_r \cos\phi_s - Pl)^2 + S^2 - R^2. \end{aligned} \tag{4}$$

The emergent point (x_e, y_e, z_e) on the lenticular surface can be calculated by substituting t obtained in Eq. (4) and the refracted angles at the base of the lens (θ_r, ϕ_r) into Eq. (3).

Figure 2 presents a schematic diagram of the optical model used in this study for finite ray tracing. The incident and emergent points on the slanted lenticular lens were converted to the corresponding points on a spherical lens in two steps: the points on the slanted lenticular were first transformed into the respective points on the non-slanted lenticular, cylindrical lens, using rotation matrix, and they were then replaced with the corresponding

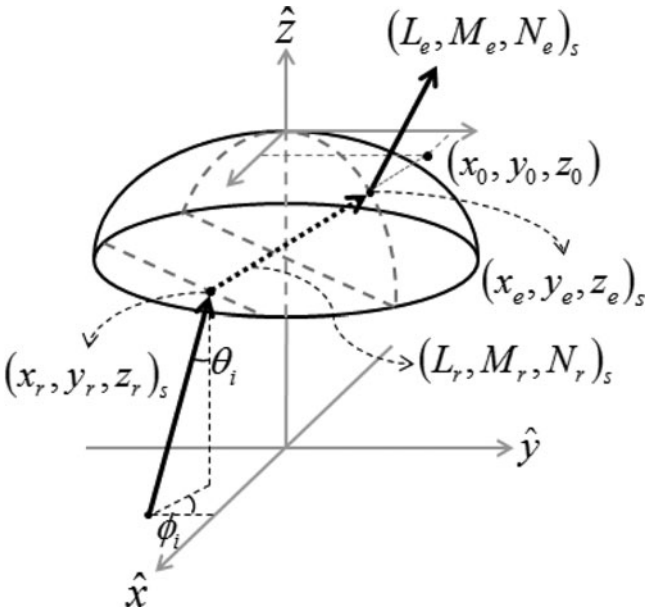

Figure 2. Schematic representation of the incident and emergent points on the spherical lens. The emergent point of the slanted lens needs to be transformed on the meridian of the spherical lens.

points on the spherical lens. The procedure can be described algebraically as follows:

$$\begin{pmatrix} x_r \\ y_r \\ z_r \end{pmatrix}_S = \begin{pmatrix} \cos\phi_s & \sin\phi_s & 0 \\ -\sin\phi_s & \cos\phi_s & 0 \\ 0 & 0 & 1 \end{pmatrix} \begin{pmatrix} x_r \\ y_r \\ z_r \end{pmatrix} - \begin{pmatrix} (t\sin\theta_r\sin\phi_r + x_r)\cos\phi_s + (t\sin\theta_r\cos\phi_r + y_r)\sin\phi_s \\ Pl\cos\phi_s \\ 0 \end{pmatrix}, \tag{5}$$

$$\begin{pmatrix} x_e \\ y_e \\ z_e \end{pmatrix}_S = \begin{pmatrix} \cos\phi_s & \sin\phi_s & 0 \\ -\sin\phi_s & \cos\phi_s & 0 \\ 0 & 0 & 1 \end{pmatrix} \begin{pmatrix} t\sin\theta_r\sin\phi_r + x_r \\ t\sin\theta_r\cos\phi_r + y_r \\ t\cos\theta_r \end{pmatrix} - \begin{pmatrix} (t\sin\theta_r\sin\phi_r + x_r)\cos\phi_s + (t\sin\theta_r\cos\phi_r + y_r)\sin\phi_s \\ Pl\cos\phi_s \\ 0 \end{pmatrix}, \tag{6}$$

where $(x_r, y_r, z_r)_S$ and $(x_e, y_e, z_e)_S$ are the incident and emergent points on the spherical lens, respectively. From Eqs. (5) and (6), the directional cosine of the light ray emerging from the spherical lens can be expressed as

$$\begin{aligned} n_{air}\,(L_e)_S &= n_{lens}\,(L_r)_S - K\,(x_e)_S, \\ n_{air}\,(M_e)_S &= n_{lens}\,(M_r)_S - K\,(y_e)_S, \\ n_{air}\,(N_e)_S &= n_{lens}\,(N_r)_S - K\,(z_e)_S + \left(\sqrt{n_{air}^2 - n_{lens}^2\left(1 - G^2 + cF\right)}\right. \\ &\quad \left. - n_{lens}\sqrt{G^2 - cF}\right), \end{aligned} \tag{7}$$

where n_{air} and n_{lens} denote the refractive indices of air and the lens, respectively. $(L_r, M_r, N_r)_S$ represents the directional cosine of the refracted light ray on the base of the spherical lens, and $(L_e, M_e, N_e)_S$ indicates that of the light ray emerging from the spherical surface of the lens. Parameters, F, G, and K, are expressed as

$$\begin{aligned} F &= c\left(x_0^2 + y_0^2\right), \\ G &= (N_r)_S - c\left((L_r)_S\,x_0 + (M_r)_S\,y_0\right), \\ K &= c\left(\sqrt{n_{air}^2 - n_{lens}^2\left(1 - G^2 + cF\right)} - n_{lens}\sqrt{G^2 - cF}\right), \end{aligned} \tag{8}$$

where the point $\left(x_0, y_0, z_0\right)$ indicates the intersection of the line extending along the direction of the light ray inside the spherical lens with the vertex plane, and c denotes the velocity of light.

The directional cosine of the light ray emerging from the spherical lens can be re-converted to that of a light ray emerging from the slanted lenticular using the following equation:

$$\begin{pmatrix} L_e \\ M_e \\ N_e \end{pmatrix} = \begin{pmatrix} \cos\phi_s & -\sin\phi_s & 0 \\ \sin\phi_s & \cos\phi_s & 0 \\ 0 & 0 & 1 \end{pmatrix} \begin{pmatrix} L_e \\ M_e \\ N_e \end{pmatrix}_S. \tag{9}$$

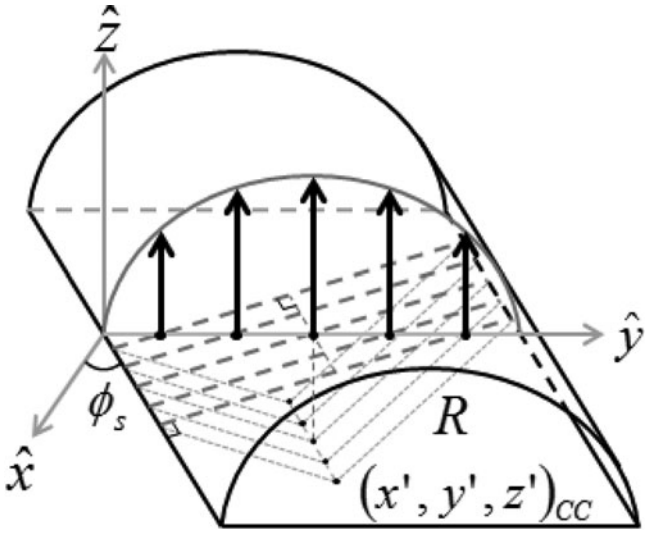

Figure 3. Schematic diagram of the normally incident light rays. The broken lines represent the intersection lines of the planes of incidence of the rays with the base of the lenticular. $(x', y', z')_{CC}$ indicates the center of curvature of the slanted lenticular.

The azimuth and inclination angles of the light ray emerging from the slanted lenticular are then given by the following:

$$\begin{aligned} \phi_e &= \tan^{-1}\left(\frac{L_e}{M_e}\right), \\ \theta_e &= \tan^{-1}\left(\frac{L_e}{\sin\phi_e}/N_e\right). \end{aligned} \tag{10}$$

Using the angles of the emergent light ray on the slanted lenticular surface given in Eq. (10), the light ray distribution for a single slanted lenticular can be obtained and three-dimensional computations can be performed by expanding the results to the entire display panel.

Simulation Results and Discussion

Figure 3 shows that the light rays are normally incident on the base of the slanted lenticular lens. Owing to the slant angle, the emergent points on the lenticular surface, where the normally incident rays arrive after passing through the lenticular, form an elliptical shape, and the centers of curvature corresponding to the respective emergent points differ from each other. In other words, each incident ray normal to the base of the slanted lenticular has a different plane of incidence due to the slant angle.

Figure 4(a) represents the computational results of the finite ray tracing for the normally incident ray described in Fig. 3. The figure shows that the azimuth angles as well as the inclination angles exist in the emergent rays. This implies that the emergent light rays from the surface of the slanted lenticular deviate from the yz-plane even though the incident light rays, perpendicular to the base of the slanted lenticular, is lying in the yz-plane. Figures 4(b) and 4(c) represent the projections of the simulation results depicted in Fig. 4(a) onto the xy-plane and yz-plane, respectively. Note that the azimuth angles at the center of the lens are reversed in sign, as shown in Fig. 4(b). In Fig. 4(c), the focal length of the slanted

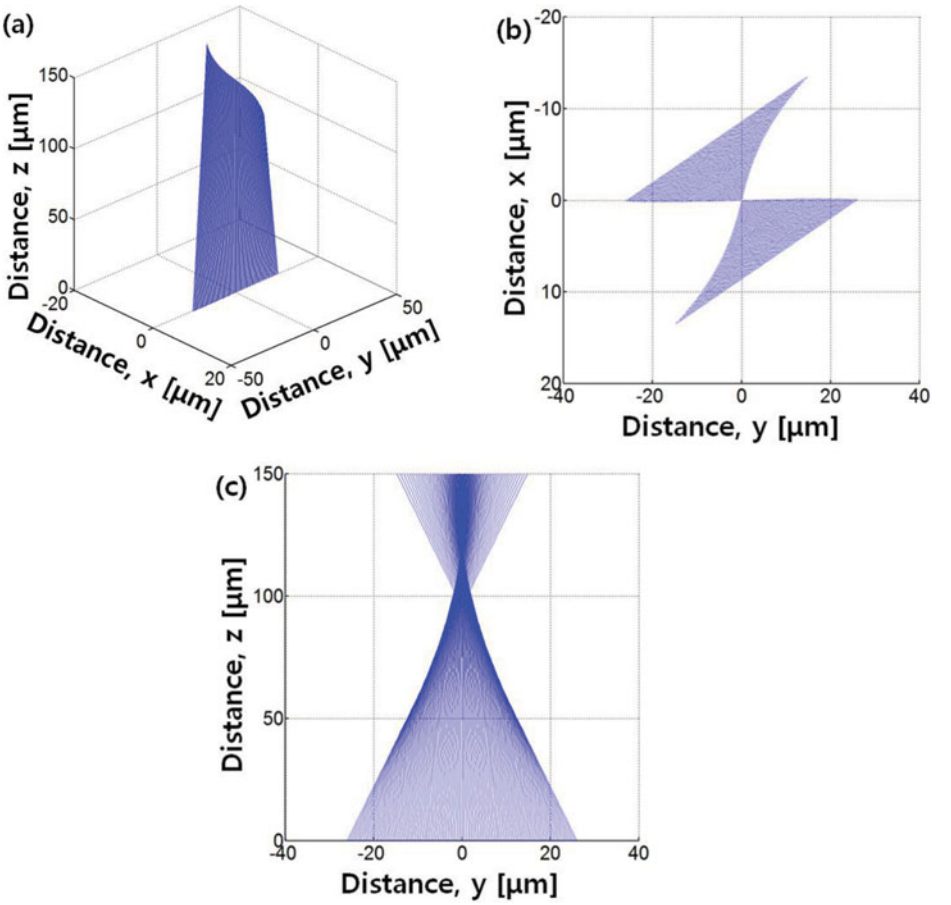

Figure 4. (a) Computational results of finite ray tracing for normally incident light rays. (b) and (c) projections of the simulation results shown in (a) onto the xy- and yz-planes, respectively.

lenticular is estimated to be 112.5 μm, which is identical to the focal length determined when designing the lenticular lens. This suggests that the results of the finite ray tracing for a slanted lenticular are identical to those for a non-slanted lenticular even though the azimuth angles are generated due to the slant angle, because the plane of incidence corresponding to each light ray incident normally can be considered a circular lens with the same curvature, size and focal length, regardless of whether the lenticular is slanted or not.

Figure 5 represents a schematic diagram of the 3D display panel with an array of slanted lenticulars. The display panel used in the simulation is a 2 view 3D-liquid crystal display with a diagonal of 4.5 $inches$. The number on the pixel means the view number that each pixel corresponds to. Each view is arranged alternately not only with the column but also with the row considering the effect of the slanted lenticular, as shown in Fig. 5. The same views are arrayed to appear together along the direction of the individual lenticular for clear separation of the left and right images at the optimal viewing distance.

Figure 6 presents the relative light intensities at the optimal viewing distance of 30 cm for each view. Figure 6(a) shows the distribution profile of the relative light intensities within a section of 50 $\times$ 50 cm^2 at the optimal viewing distance. The images for the

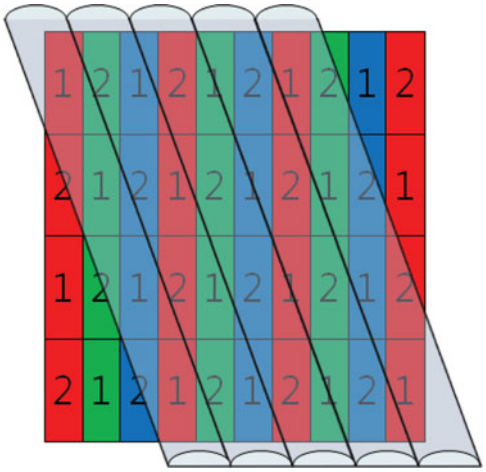

Figure 5. Schematic diagram of a 3D display panel with an array of lenticulars. The number on the pixel means the view number that each pixel corresponds to.

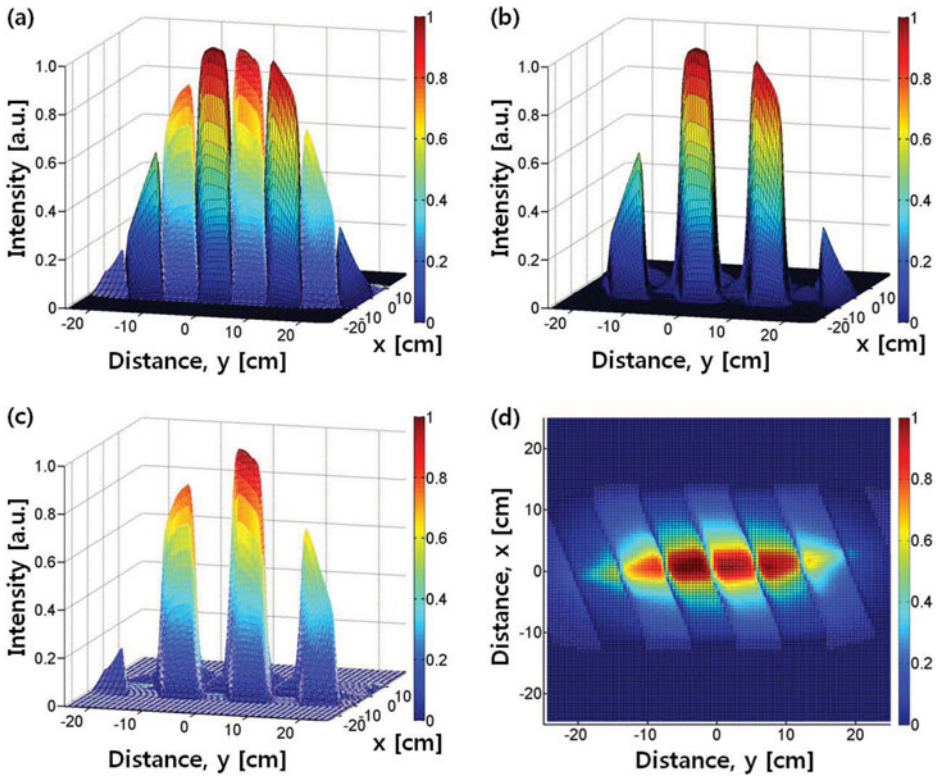

Figure 6. Relative light intensities at the optimal viewing distance of 30 *cm* for each view: (a) the distribution profile of the relative light intensities within a section of 50 × 50 cm^2. The solid and dotted lines indicate the images for the left and right eyes. (b) and (c) relative light intensities of the images for the left and right eyes, respectively. (d) projection of (a) onto the xy-plane.

left and right eyes, which are represented by the solid and the dotted lines, respectively, are distributed alternately and the image at the center of the section has the maximum light intensity, as expected. For convenience, the images for the left and the right eyes are represented separately in Figs. 6(b) and 6(c). Approximately 5% noise exists between the two images. The noise cannot be interpreted in a two-dimensional simulation, whereas it can be obtained in the present work by considering the influence of the slant angle. The slant angle causes the plane of incidence to be inclined by that angle, leading to noise between the images for the left and right eyes. Figure 6(d) shows a projection of Fig. 6(a) onto the xy-plane. As shown in the figure, the shape of the viewing zone at the optimal viewing distance is tilted towards the direction of the slanted lenticular. The distance between the centers of each view is in good agreement with the inter-ocular distance, 65 mm.

Conclusion

In the present study, a three dimensional simulation was carried out using the geometrical optics and some algebraic calculations to investigate the optical functionalities of an autostereoscopic display with an array of lenticular lenses. Prior to the simulation, the specifications of the lenticular lens were determined by considering the resolution of the display panel, the size of a pixel, the configuration of pixels, the number of views, and so on.

A numerical simulation was carried out by expanding the simulation results for a single lenticular to the entire display panel. As a first step to perform finite ray tracing for a single lenticular, we calculated the path of light travelling inside the slanted lenticular using Snell's law. Based on the results obtained, the emergent point on the slanted lenticular surface was calculated using the modified equation of a cylinder. The incident and emergent points on the slanted lenticular lens were then converted to the respective points on the spherical lens in two steps: the points on the slanted lenticular were first transformed into the respective points on the non-slanted lenticular, cylindrical lens, using rotation matrix, and they were then replaced with the points on the spherical lens. Finite ray tracing was then performed to obtain the directional cosines of the emergent rays. By reconverting the obtained directional cosines into those of the original coordinates using a reverse rotation matrix, the directional cosines of the emergent light rays from the slanted lenticular surface were finally obtained. Based on the results, the relative light intensities at the optimal viewing distance according to the incident angles were then calculated.

As a result, each view was confirmed to be located at the inter-ocular distance, 65 mm, away from each other. Approximately 5% noise existed between the views. The noise could not be interpreted in the two-dimensional simulation, whereas it could be obtained by considering the influence of the slant angle. The slant angle causes the plane of incidence to be inclined by that angle, thereby generating noise between the views. The shape of the viewing zone at the optimal viewing distance was tilted towards the direction of the slanted lenticular. The simulation method presented in this study will enable a realistic evaluation of the optical functionalities, such as the shape of the viewing zone, of autostereoscopic displays with an array of lenticulars.

Funding

This study was supported by an Inha University research grant.

References

[1] Benton, S. A. ed. (2001). *Selected Papers on Three-Dimensional Displays*, SPIE Optical Engineering Press: Bellingham, WA.
[2] McAllister, D. F. ed. (1993). *Stereo Computer Graphics and Other True 3D Technologies,* Princeton Univ. Press: Princeton, NJ.
[3] Okoshi, T. (1976). *Three-Dimensional Imaging Techniques*, Academic Press: London, UK.
[4] Park, M. C., Lee, H. D., & Son, J. Y. (2011). *Proc. International Display Workshops*, 1849.
[5] Jung, S. M., Jang, J. H., Kang, H. Y., Lee, K. J., Kang, J. N., Lee, S. C., Lim, K. M., & Yeo, S. D. (2013). *Proc. SPIE*, *8648*, 864805.
[6] Jung, S. M., Lee, S. C., & Lim, K. M. (2013). *Curr. Appl. Phys.*, *13*, 1339.
[7] Lin, P. D., & Tsai, C. Y. (2012). *J. Opt. Soc. Am. A*, *29*, 174.
[8] Miks, A., & Novak, A. (2012). *J. Opt. Soc. Am. A*, *29*, 1356.
[9] Lin, P. D., & Tsai, C. Y. (2012). *J. Opt. Soc. Am. A*, *29*, 1358.
[10] Berkel, C. V., & Clarke, J. A. (1997). *Proc. SPIE*, *3012*, 179.
[11] Berkel, C. V., Franklin, A. R., & Mansell, J. R. (1996). *Proc. Euro Display' 96*, 109.